EPJ Photovoltaics **15**, 19 (2024)

https://doi.org/10.1051/epjpv/2024017

Available online at:
www.epj-pv.org

Special Issue on 'EU PVSEC 2023: State of the Art and Developments in Photovoltaics', edited by Robert Kenny and João Serra

ORIGINAL ARTICLE OPEN ACCESS

Investigation of perovskite layer growth from solution on textured substrates

Florian Riesebeck*, Florian Mathies, Danbi Yoo, Sergei Trofimov, Eva Unger, and Christiane Becker

Helmholtz-Zentrum Berlin für Materialien und Energie, Hahn-Meitner-Platz 1, 14109 Berlin, Germany

Received: 20 September 2023 / Accepted: 9 April 2024

Abstract. Surface textures are indispensable to minimize optical losses in perovskite-based solar cells. However, the solution-processing of perovskite layers is often not compatible with textured substrates, and little is known about the film growth thereon. This study aims to elucidate the growth process of perovskite layers from solution on textured substrates and to identify the texture features ensuring compatibility with perovskite solution-processing. Using nanoimprint-lithography we prepared three different periodically as well as randomly textured glass substrates for spin-coated perovskite solar cells, of which one was duplicated from a commercially available texture. During the perovskite crystallization process, a time-resolved in situ photoluminescence measurement was conducted. The photoluminescence signal was not found to substantially alter using textured substrates with texture heights around 500 nm. Optical absorptance spectroscopy and scanning electron microscopic imaging were applied to investigate the growth, crystal structure, and optical properties of solution-processed perovskite on top of different textures. We find that periodic textures with height around 500 nm enable homogeneous solution-processed perovskite layers with optimized optical performance. In contrast, texture heights of several micrometers lead to macroscopic holes in the perovskite film. The results of this study will help to find optimum optical textures for high-efficiency perovskite single-junction and perovskite-silicon tandem solar cells.

Keywords: Perovskite / textures / in-situ photoluminescence / nanoimprintlithography / optics for solar cells

1 Introduction

Combining perovskite based solar cells with conventional silicon solar cells in a tandem cell setup enables higher efficiencies due to covering a higher range of wavelengths in the solar spectrum. Perovskite-silicon tandem solar cells have strongly advanced and recently even reached 33.9% efficiency [1]. To fully exploit the efficiency potential of this technology, textured interfaces are required to minimize optical losses. These textures must be compatible with the processing of perovskite, which is challenging, particularly when the perovskite is processed from solution. Pioneering works in monolithic perovskite-silicon tandem solar cells used silicon bottom cells with a nanopyramidal surface texture and successfully combined them with a blade-coated [2] or spin-coated [3] perovskite top cell. It was also shown that perovskite solar cells can be fabricated via spin-coating on various other textured substrates, such as periodic sinusoidal nanotextures and inverted pyramids, without deterioration of the electronic performance [4]. Later, we showed that the implementation of sinusoidally nano-textured interfaces enables 29.8% efficiency in perovskite-silicon tandem solar cells by not only reducing optical losses but also improving the optoelectronic properties in terms of open-circuit-voltage and increasing the fabrication yield by improved wetting of the perovskite on textures [5]. The interplay between perovskite solution processing and texture silicon bottom cell received more attention [6]. A non-ideal wetting of perovskite precursor solution was found to be an issue particularly if self assembling monolayers (SAMs) are used, as reported by various groups in the recent past [7–10]. However, several studies have also been published indicating a better wettability of the perovskite solution and a better layer growth if a textured substrate was used [5,11,12]. While the correlation between textures and reduced optical losses is well understood, there are only a few works investigating the in-situ perovskite layer growth from solution on textured surfaces. Here in this study, we investigate the perovskite layer growth from solution on textured substrates using in-situ photoluminescence (PL) measurements and various microscopic characterization techniques.

2 Experimental

2.1 Nanoimprint lithography

The texturing of the glass substrate covered by a resist layer is done by nanoimprint lithography (NIL), as structuring substrates with conventional lithography

* e-mail: florian.riesebeck@helmholtz-berlin.de

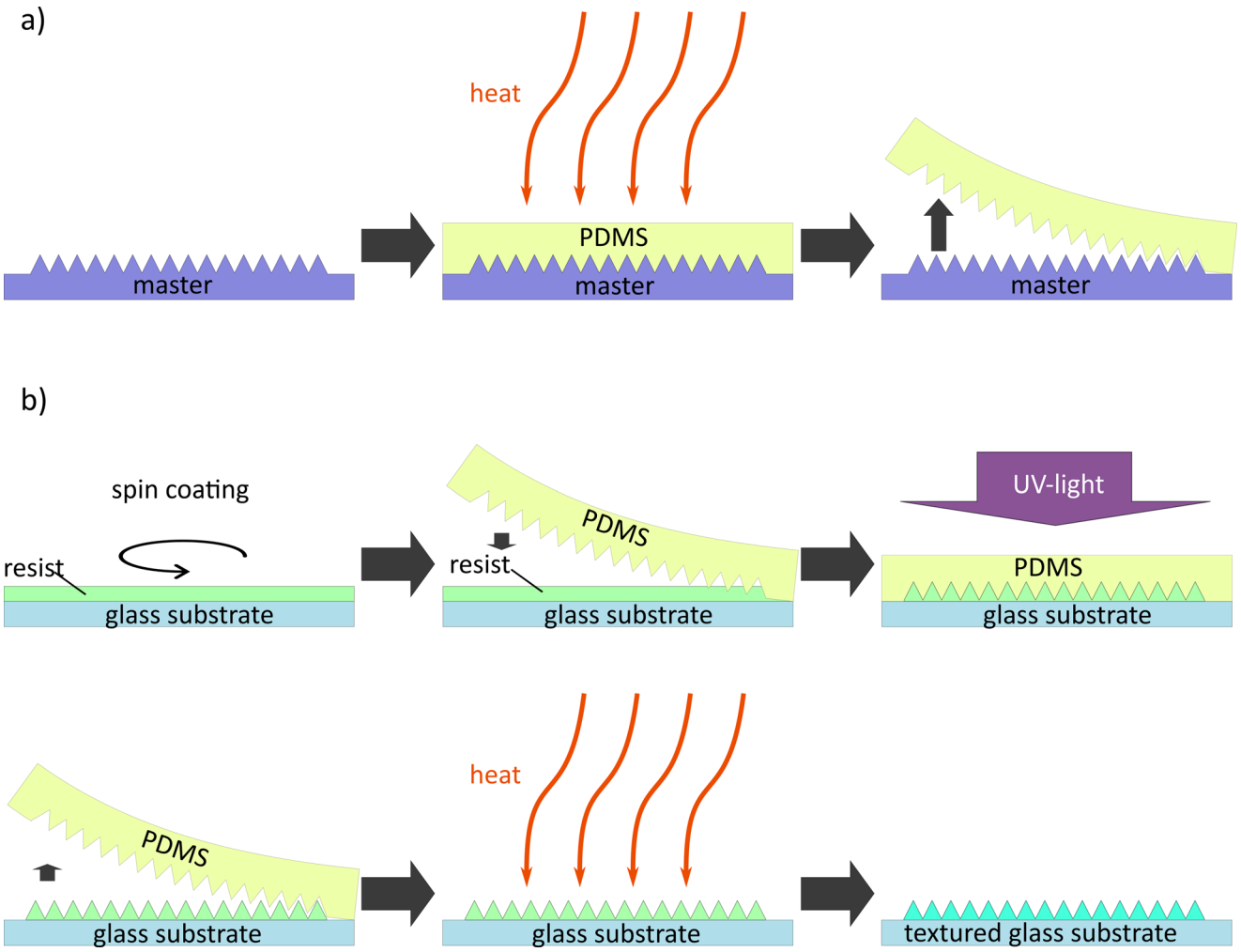

Fig. 1. Fabrication of textured glass substrates using nanoimprint lithography. (a) Replication of the master structure in an inversed PDMS-stamp. (b) Processing steps needed to transfer the inverted texture of the stamp into the resist on the substrate.

methods is very time- and cost intensive. The NIL-process enables lithography with a resolution down to 5 nm while keeping the costs low and the output volume high.

The NIL-process starts with a so-called "master structure" that has the desired texture, which has been produced by other lithography processes such as interference lithography or photolithography or a combination of different methods.

First, an inverted version of the master structure is prepared using a polydimethylsiloxane (PDMS) polymer. For this purpose, a commercially available PDMS polymer precursor and a suitable catalyst are mixed in a ratio of 9:1 and degassed through a desiccator to avoid air entrapment in the later stamp. Figure 1a shows how the viscous PDMS is then poured onto the master structure and thermally annealed at 70 °C for 30 min. Subsequently, the negative stamp can be removed from the master structure without leaving any residue. Since this is a non-destructive process, the original structure remains intact, allowing the process to be performed multiple times as needed. The stamp can now be used in the second process step to transfer the structure to any substrate. The substrates used in this work are $5 \times 5\ \mathrm{cm}^2$ of Schott T-eco 264® glass with a thickness of 1.1 mm covered by a UV-hardening resist. Here we use the hybrid polymer OrmoComp® (Micro Resist Technologies), which is mixed with the thinning agent OrmoThin® (Micro Resist Technologies) in a ratio of 1:2 to adjust the film thickness. With this ratio, a film thickness of $\approx 1\ \mu\mathrm{m}$ is achieved.

Usually, a layer thickness in the height of the texture is sufficient. However, since different textures with different texture heights are processed in this work, a uniform thickness of the resist layer is chosen for comparison purposes. This has no difference in the optical properties of the material. Figure 1b shows the steps to transfer the inverted texture in the stamp to the substrate. The resist is applied to the glass substrate in a spin coating process at 3000 rotations per minute (rpm) for 30 s. Afterward, the substrate must be heated for 2 min at 80 °C on a hotplate in a pre-bake process to remove any remaining solvents after spin coating. The stamp is now carefully rolled onto the target substrate with the aid of a metal cylinder and pressed in. For curing, the stack of substrate, resist and stamp is illuminated for 5 min under a commercial UVB broadband lamp. PDMS is a transparent polymer, which allows the curing of the underlying resist. The PDMS stamp is then carefully removed from the substrate. The stamp can be used for up to ten substrates before a new stamp is recommended.

2.2 Hole transport layer

To ensure the results are applicable to real solar cell applications, a well-known stack previously utilized for tandem perovskite-silicon solar cells was employed to demonstrate its transferability. The first layer after the texturing is an indium-tin-oxide (ITO) layer that is RF sputtered from a ceramic target with 0.2% oxygen in the Ar/O_2 sputter gas mixture in a sputtering tool from Roth&Rau. For this work a sputtering process was chosen that would produce a layer of thickness of 150 nm on a planar substrate. The sputtering process was conducted at room temperature and with a rotating sample holder underneath the sputter target to ensure an even ITO layer. Due to the different surface enhancement factors the actual layer thickness of the ITO varies depending on the texture. Since the goal was not to produce a properly working solar cell this does not pose any difficulties. Afterwards, 100 µl of a 1 mM solution of MeO-2PACz molecule dissolved in ethanol was spin-coated for 30 s at 3000 rpm with a windup time of 5 s and afterwards cured for 10 min at 100 °C to bond it to the surface and evaporate remaining solvents. This self-assembling-monolayer (SAM) works as a hole transport layer [13].

2.3 Perovskite layer

After the preparation of the substrates with NIL, and the application of an ITO and SAM layer, the perovskite layer is deposited in a solvent-based spin-coating process. The $Cs_{0.05}(FA_{0.83}MA_{0.17})_{0.95}Pb(I_{0.83}Br_{0.17})_3$ perovskite was prepared following Saliba et al. [14] by mixing precursor solutions containing formamidinium iodide (FAI) and lead iodide (PbI_2), as well as lead bromide ($PbBr_2$) in the ratio of 5:1. The precursor contained 1 M of the organic and 1.1 M of the lead salts and was dissolved in anhydrous dimethyl formamide/dimethyl sulfoxide (DMF/DMSO) 4:1 (v/v). Further on, 5% vol cesium iodide (CsI) from a 1.5 M stock solution in DMSO was added to the precursor solution. The ink is then spin-coated in a two-step program at 1000 rpm for 10 s and afterward with 6000 rpm for 20 s. 15 seconds after the beginning of the spin coating, 250 µl of anisole was deposited onto the spinning substrate as an antisolvent drop. During the PL measurements, the second step duration was increased to 45 seconds. This was done to further visualize the PL data over a longer time and get PL data even after the actual formation of the film. This was necessary, as the PL setup was specifically designed for measuring during spin coating opposed to a conventional PL setup. After the spin coating, the substrates were hard-baked for 30 min at 100 °C to remove all the leftover solvents.

2.4 Characterization

In order to display the investigated textures with feature size around and below one micrometer, that were used in this work, atomic force microscopy (AFM) measurements of the textured substrates were conducted in a non-contact mode on a Park Systems NX12 device using 160AC-NA (OPUS by MikroMasch) cantilevers. The Gaussian Circular Diffusor texture with micrometer sized features was imaged with a Keyence VK-X 200 confocal laser scanning microscope (CLSM).

After measuring the PL spectrum during crystallization, the substrates with the newly deposited perovskite layer are imaged using a LEXT OLS5100 3D laser scanning microscope (Olympus) in optical imaging mode at 50x magnification. To get an overview of the whole surface, the substrates are scanned in a 5×5 grid and images are taken at the respective positions. Unlike the SEM, these images do not yet show the crystal structure on the surface. However, they can be used to make an initial assessment of whether the perovskite has formed a conformal coating and count the pinholes that might have formed during crystallization.

For further characterization, a UV/Vis/NIR spectroscopy measurement was conducted using a Perkin Elmer Lambda 1050+ UV/Vis/NIR spectrometer. The reflection, as well as the transmission of the produced samples, were then measured in a wavelength range between 250 nm and 1200 nm in 5 nm steps. Since the sum of transmission, reflection and absorptance always equals 100%, the absorptance could then be determined from the values obtained.

To visualize the perovskite growth on the textured layers, the substrates were examined under the scanning electron microscope. Both cross-sectional and top views were taken of the samples for this purpose.

3 Results and discussion

3.1 Surface textures

In this work, three different substrate textures (Fig. 2) were investigated and compared to a planar reference. The first texture is a sinusoidal texture with a peak distance of around 750 nm (manufacturor's information) and a texture depth of 300. The second texture is a periodic structure consisting of inverted pyramids with a periodicity of around 1250 nm (manufacturor's information), a depth of around 500 nm and a pyramid base of 1000 nm. The last structure examined is a commercially available Gaussian circular diffusor texture, produced in foils by the company temicon GmbH. This diffusor has a vertical feature size of $1.6\,\mu m \pm 0.2\,\mu m$ and a horizontal distance between features of 10–30 µm. The sinusoidal and inverted pyramidic textures were chosen as their compatibility with high quality perovskite solar cell processing via spin-coating had been proven in the past [4,5]. The Gaussian circular diffusor texture had been added to the portfolio to investigate if its smoothness and large-area compatibility might be beneficial solution processed perovskite solar cells. The texture parameters were determined by a minimum of 16 measurement points with corresponding standard deviations provided in Table 1. AFM was deployed for its high z-axis resolution capabilities in nano-scale texture analysis, while CLSM was selected to overcome the z-axis limitations of AFM for larger micro-scale texture characterization.

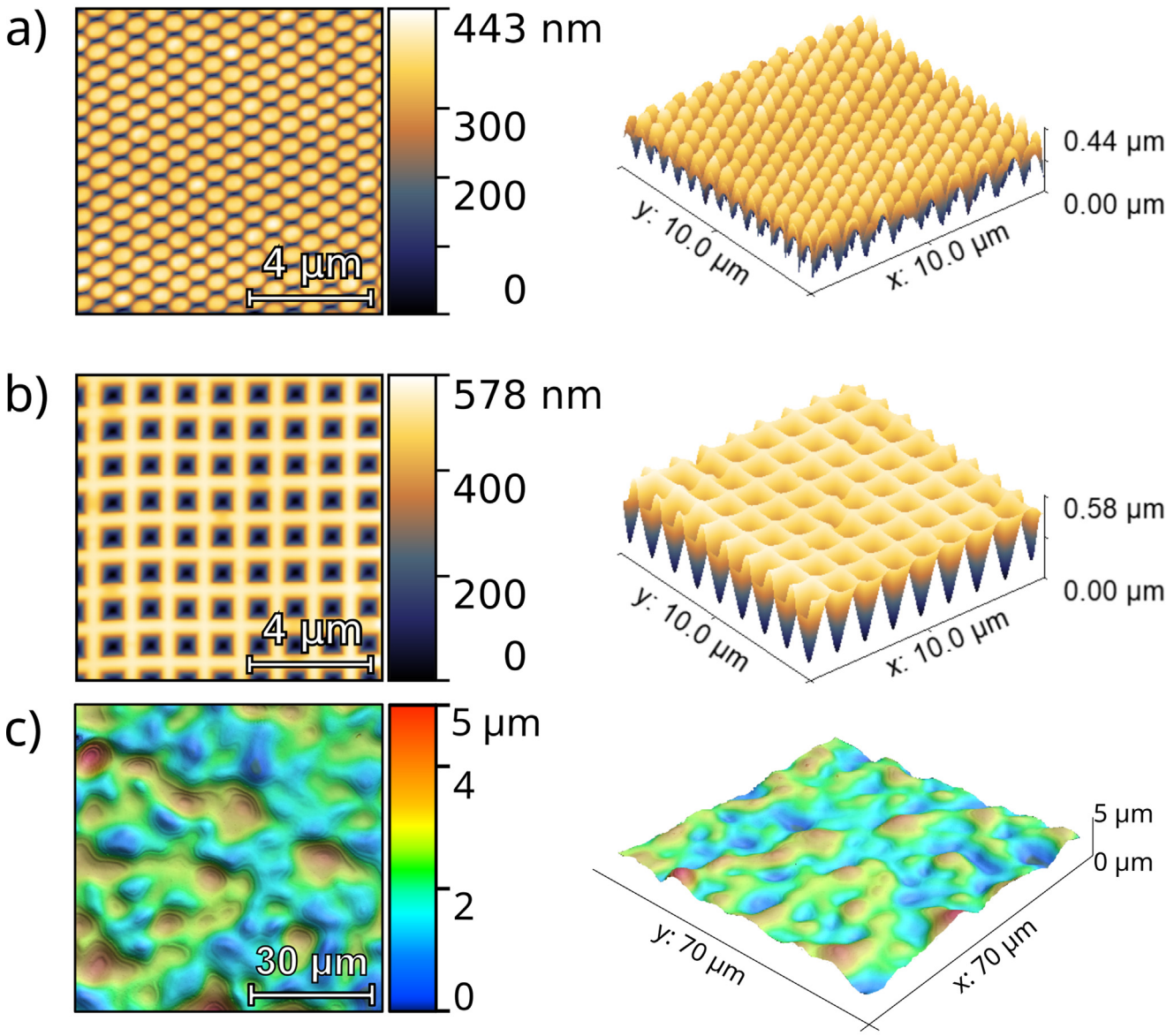

Fig. 2. Atomic force (a and b) and confocal laser (c) microscope images of the three textures investigated in this study. (a) Sinusoidal texture in hexagonal geometry, with peak distance and texture depth of around 750 nm (manufacturer's information) and 300 nm, respectively. (b) Periodic inverted pyramids with periodicity and depth of around 1250 nm (manufacturer's information) and 500 nm, respectively, and a base side length of 1000 nm. (c) Commercially available Gaussian circular diffusor texture, produced in foils by temicon GmbH, Germany.

Table 1. Summary of structural properties of the textures investigated in this study as extracted from atomic force microscopy (sinusoidal and inverted pyramidal texture) and confocal laser scanning microscopy (diffusor) measurements.

Texture	Lattice geometry	Peak-to-peak distance p	Peak-to-valley height h	Surface enhancement factor
Planar reference	–	–	–	1
Sinusoidal	Hexagonal	(734 ± 22) nm	(297 ± 10) nm	1.36
Inverted pyramids	Square	(1191 ± 26) nm	(504 ± 8) nm	1.3
Gaussian circular diffusor	Random	(10.6 ± 3.7) µm	(1.6 ± 0.2) µm	1.3

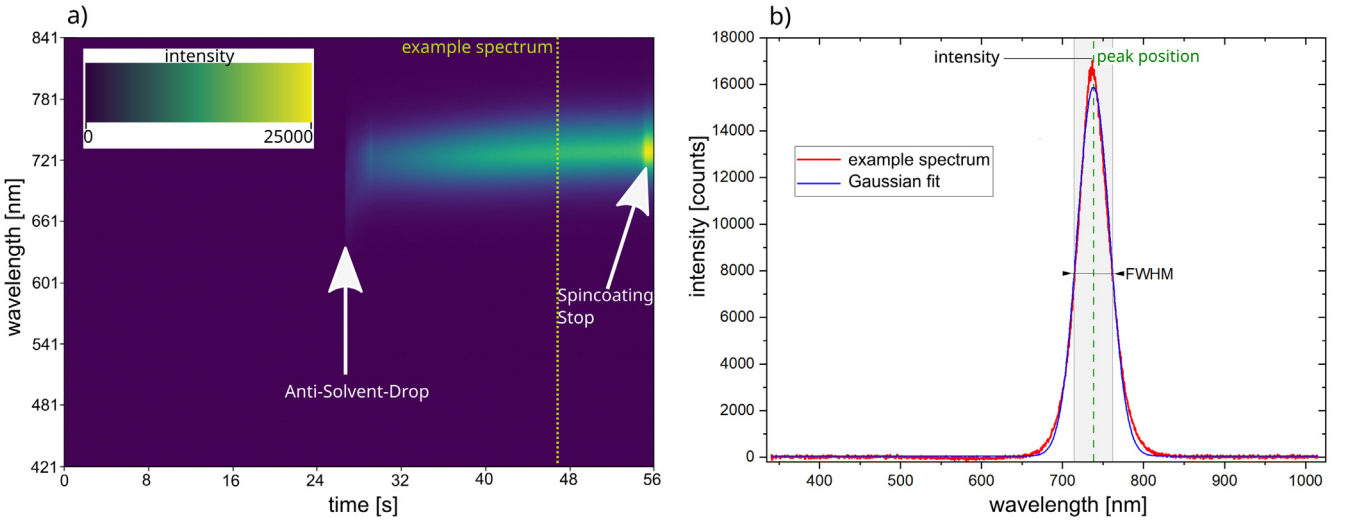

Fig. 3. (a) Heat map of the photoluminescence (PL) measurement of the planar perovskite reference film. After 25 seconds of spin-coating of the perovskite precursor solution, the antisolvent-drop was added. (b) Example PL spectrum taken at 47 seconds of the map shown in part (a) (dashed line) to visualize the parameters PL peak position, full width at half maximum (FWHM) and intensity.

3.2 In situ photoluminescence

During the deposition of the perovskite layer, the photoluminescence signal was measured in time steps of 0.5 s in the wavelength range between 250 nm and 1050 nm. Plotting the recorded spectra over time creates a heat map (Fig. 3a) visualizing the formation process of the wet perovskite film onto the substrate. We see a PL-signal onset after 25 s that is consistent in time with setting antisolvent drop. The intensity of the PL signal changes over time to higher intensities and longer wavelengths, as expected from the perovskite growth process of triple cation perovskites [15].

Figure 3b shows an example spectrum taken at 47 s of the map shown in part (a) (dashed line). The red curve shows the actual measured intensity of the spectrum. The background radiation of the measurement was calibrated before the start of the measurement, so the background noise was offset to get more clear data. To analyze the data, a Gaussian fit is applied to each of the recorded PL spectra (blue curve). This filters out the noise of the measured values from the results. From this fit, the peak position and the full width at half maximum (FWHM) of the recorded spectrum can be calculated.

As soon as the antisolvent drop is released, a yellowish haze can be seen on the heat map. The more a point moves towards yellow, the higher the measured intensity of the PL spectrum at that point.

Since a Gaussian fit has been performed on each time-resolved spectrum recorded, the position of the peak is also known at each time point. Accordingly, a curve of peak position, full width at half maximum (FWHM) and the peak intensity over time can be displayed for each measured textured substrate. Figure 4a shows this curves for all textured surfaces examined shortly after the time of adding the antisolvent drop, which is added after exactly 25 s of the spin-coating process. Shortly after the drop is added, the formation of the perovskite begins.

It can be seen in Figure 4a that the course of the position of the peak is very similar for all textured substrates. Likewise, all textures show a start of crystallization with a peak position around 710 nm ± 5 nm. A fast shift in the position of the PL peak from 710 nm to 725 nm within 3 seconds is seen, which we refer to the growth of perovskite crystallites, initiated by the antisolvent-drop. At the end of the measurement the peak wavelength is around 741 nm ± 1.5 nm, which is in line with other published triple cation data [16]. Due to the lower DMF content and the increasingly progressive crystallization of the perovskite, the peak of the PL spectrum shifts to higher wavelengths between 739 nm and 742.5 nm. Since the measurement is started manually and the antisolvent drop is added by hand, an error in the time of addition of the antisolvent drop to time of ± 1 s is assumed. It can be seen that the perovskite layers on all textures show the first peaks in the PL measurement at the time of 26.5 s ± 0.5 s, i.e. they start to crystallize. There are no remarkable differences between the different textures regarding PL starting time and PL peak position at the end, only the curve of the Gaussian circular diffusor (green dash dotted line) varies in its trajectory.

Another way to illustrate the crystallization of perovskite on different textured substrates is the full width at half-maximum (FWHM) value (Fig. 4b). This value can be used to show whether the width of the peak changes over time. In the specific case of the PL measurement, higher wavelength and smaller FWHM values correspond to bigger and more similar crystallites. As with the PL peak positions, the FWHM can also be shown as a time-resolved curve for the different textures examined. Figure 4b shows the course of the half-widths of the PL measurement during the spin coating of the perovskite layer onto the different textured substrates. With the deposition of the antisolvent drop a first crystallization of the perovskite layer occurs with smaller crystallites, recognizable in the lower wavelength peak and

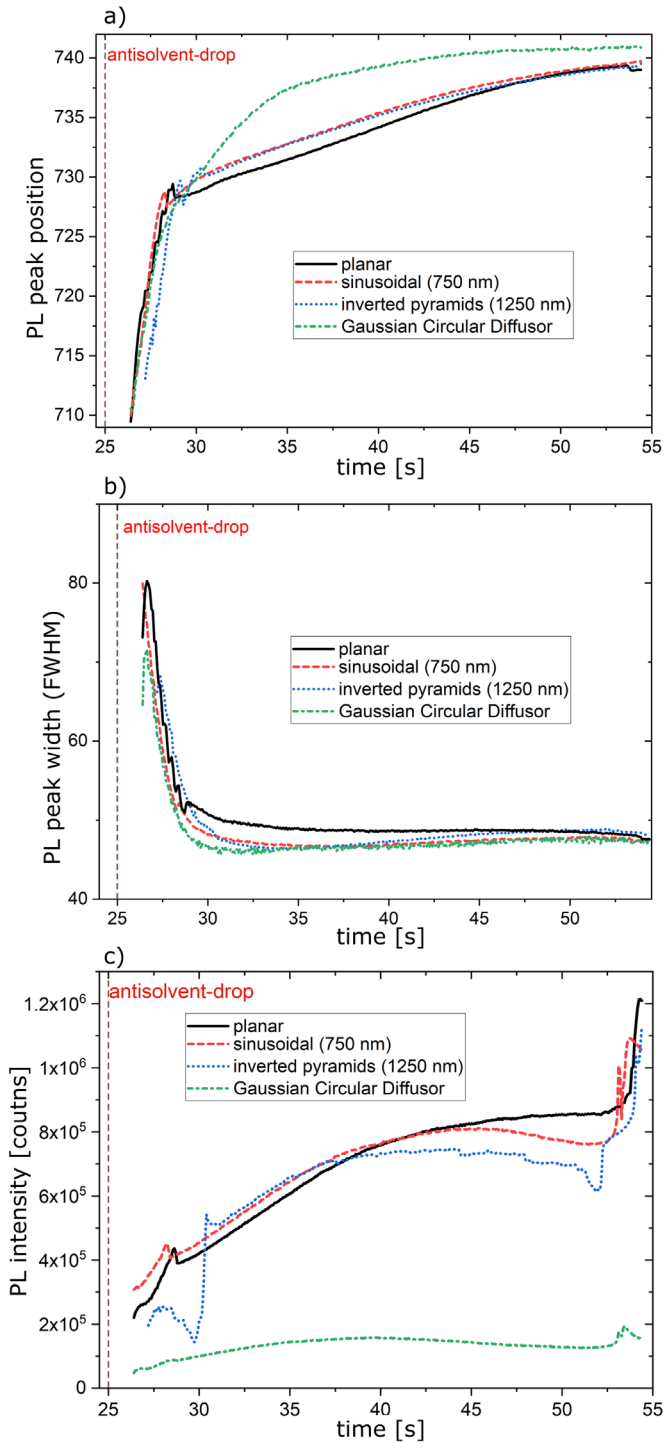

Fig. 4. (a) Center position, (b) full width at half max (FWHM), and (c) intensity of the PL peak over time right after the deposition of the antisolvent drop.

wider FWHM values. Due to the still remaining solvents in the film, these first crystals are being dissolved again only to reform into bigger and more similar crystallites, recognizable in the higher wavelength peak closer to the desired perovskite bandgap and the narrower FWHM values ≈ 3–5 s later. Here, for all substrates, the half-width drops to 48 nm ± 2 nm and remains close to this value until the end of the measurement.

Due to the PL measurement being in-situ, we average the rotations of the spin coater, thus we also average locally over a large area. The measured signal intensity (Fig. 4c) of the perovskite deposition on the sinusoidal structure (red dashed line) and the inverted pyramidal structure (blue dotted line) resembles the measurement of the planar reference (black solid line) until 40 s, with the intensity slightly decreasing afterwards. The increase of the signal after 52 s arises from the stop of the spin-coating process and will not be considered here. In contrast, the PL intensity of perovskite on the Gaussian circular diffusor (green dash dotted line) strongly deviates from the respective values of the planar reference with almost a factor of 7 lower values. The reasons for the lower PL intensity can be manifold, for example a lower coverage of the substrate with perovskite, PL light being scattered away from the detecting fiber, and quenching of the PL by non-radiative recombination channels. Disassembling the different contributions will be a topic of future work.

Summarizing the in situ PL measurements, there is no indication for a substantially different crystallization behavior of spin-coated perovskite films on planar substrates and on the investigated sinusoidal and inverted pyramid textured substrates with texture feature sizes of around one micrometer. The PL data of spin-coated perovskite films on the Gaussian circular diffusor texture indicate a quite different crystallization behavior. In the following paragraphs, possible reasons for that will be analyzed.

3.3 Scanning electron microscopy

To visualize more precisely how the perovskite is finally crystallized on the textured substrates, the layer stacks are viewed in a cross-section and a top view under the scanning electron microscope (SEM).

The cross-section view is a very good way of displaying the individual layers of the layer stack. Just before the image is taken, the back of the substrate is scored with a glass cutter and then broken at the edge. Figure 5a shows the cross-sectional view of the planar reference substrate. All layers of the layer stack deposited on the glass substrate are visible, with exception of the SAM, as it is a monolayer and therefore cannot be seen in SEM images. The lowest layer is the imprint resist with a thickness of around 1.5 µm. Directly above is the slightly lighter ITO layer followed by the perovskite film. In case of the sinusoidal (Fig. 5b) and the inverted pyramidal (Fig. 5c) textures the perovskite has filled the valleys of texture and created a surface like that of the perovskite layer on the planar substrate. On the Gaussian diffusor texture, the perovskite film is very unevenly distributed on the texture and there are different layer thicknesses at all places where the layer was formed. As the sample break is not directly crossing tips and valleys of the inverted pyramidal structure (Fig. 5c) the cross-section image gives the impression that the ITO has not conformally coated. However, previous

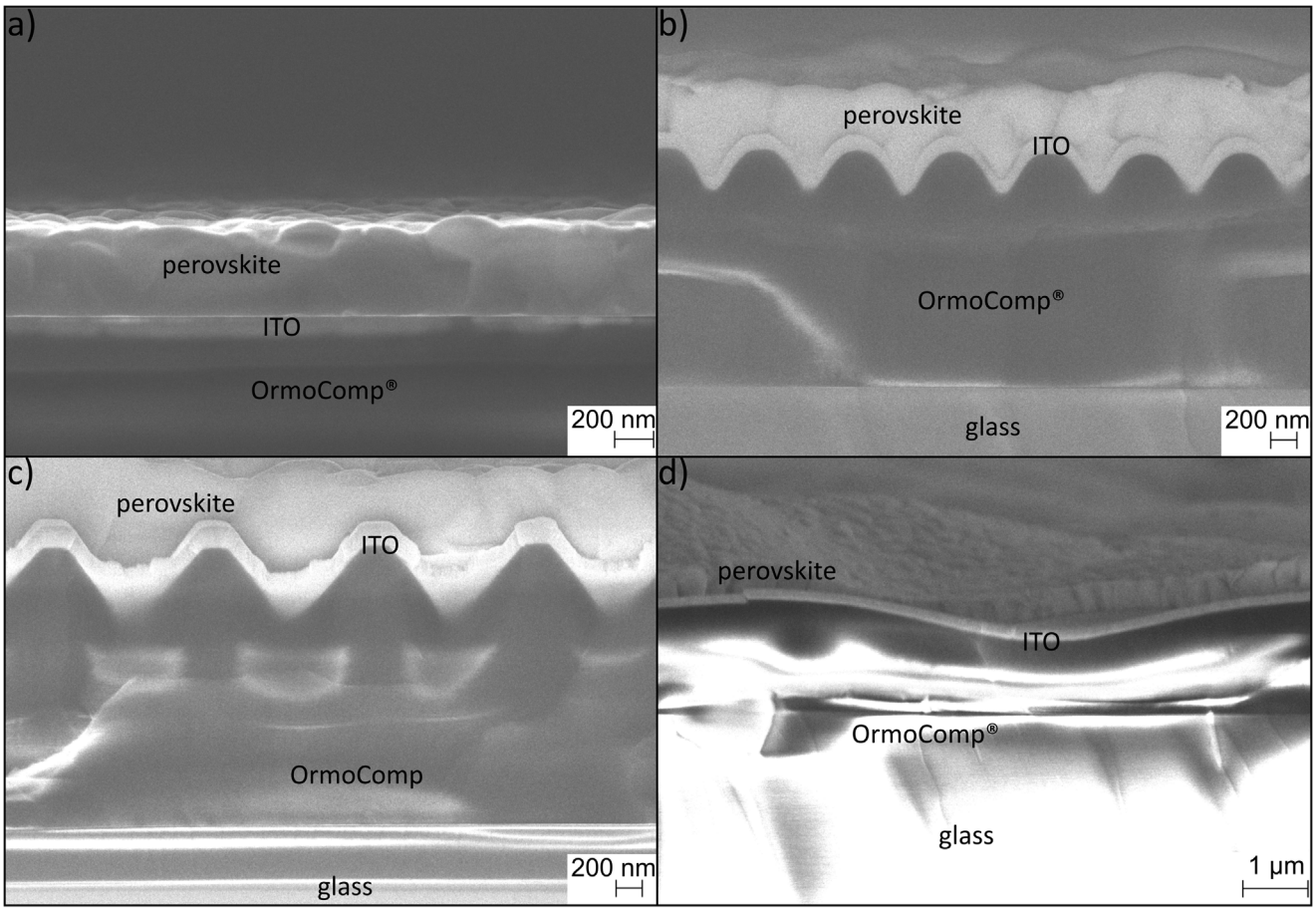

Fig. 5. Cross-section SEM images of a perovskite/SAM(not visible)/ITO layer stack on differently textured substrates. (a) Planar reference, (b) sinusoidal texture, (c) inverted pyramids, and (d) Gaussian circular diffusor.

studies indicate that the ITO coating should be nearly conformal [4]. Under the SEM the crystal structure of the perovskite with the individual crystals can be seen.

The surface of the grown perovskite layer is shown in Figure 6a with a top-view image for the planar reference substrate. A typical surface structure of perovskite can be seen. The perovskite layer consists of many single crystals crystallized together to form a closed and conformal layer. Table 2 shows the results of a grain size analysis from the SEM images shown in Figure 6. The determined grain sizes are in a similar range for all substrates with a tendency for larger grains if a textured substrate is used. In Figures 6b and 6c growth artifacts can be seen on top of the sinusoidal as well as the inverted pyramidal structure. These artifacts could be so-called dendritic structures originating from an intermediate phase of the DMF [17]. As there are no additional peaks or shoulders in the PL measurements, we assume that these structures have no optical influence on the PL measurements. As these structures are not visible in the cross cross-section, it could be assumed that they are a rather thin layer and don't influence the growth of the perovskite below it. Nevertheless, irregularities in the perovskite film are undesirable and should be avoided if possible. If the structures are dendritic, the cause is a not optimally adjusted antisolvent drop or a not yet optimized solution composition. Holes in the texture of the Gaussian diffusor are visible under the SEM (Fig. 6d) and under the optical microscope (Inset). The holes in the texture have round shapes and are distributed throughout the perovskite film. The texture has heights in the micrometer range, but due to the particularly flat slopes within the texture, one might have expected a particularly well-grown perovskite film. The much lower PL intensities measured on the perovskite film grown on Gaussian diffusor texture (Fig. 4c) cannot be fully explained by the macroscopic holes and the non-complete coverage of the film. Further reasons might be scattering of the light by the texture and/or a higher share of non-radiative recombination in the film. To differentiate the impact of texture induced light scattering and reduced electrical material quality further experiments are necessary.

3.4 Optical spectrometry

The most important optical parameter for a solar cell is the absorptance in the perovskite layer, which directly correlates with the energy yield. Figure 7 shows the absorptance (A) spectra for the selected textured substrates compared to the spectrum of the planar reference substrate after perovskite deposition. These values were

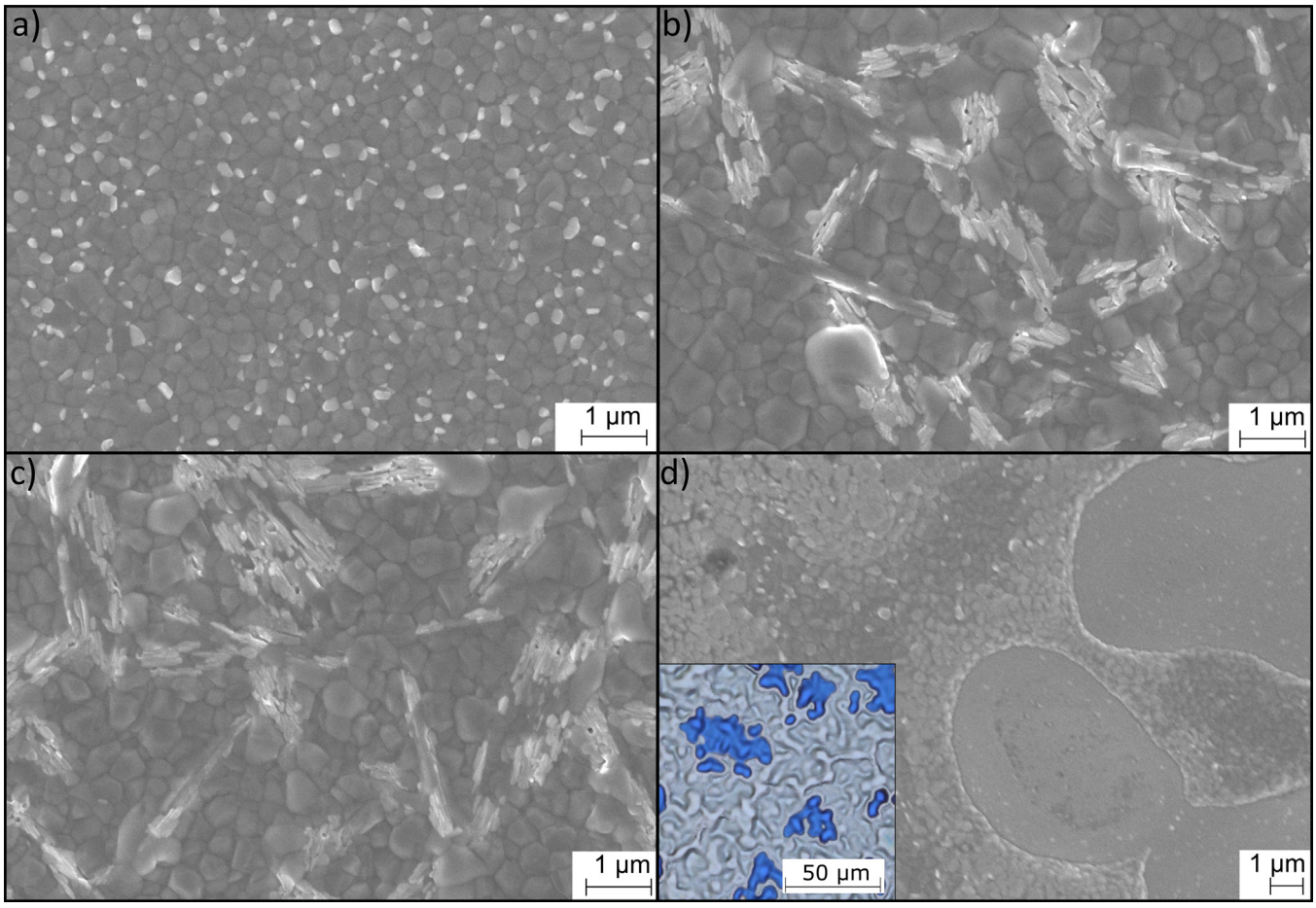

Fig. 6. Top-view SEM images of perovskite films grown on the different textures (a–d). (a) Planar reference, (b) sinusoidal texture, (c) inverted pyramids, and (d) Gaussian circular diffusor. The inset in (d) shows a larger area of the latter taken by optical microscopy.

Table 2. Grain size analysis of the perovskite layer on different textures.

Texture	Maximum grain size	Minimum grain size	Mean grain size
Planar reference	668 nm	107 nm	308 nm
Sinusoidal	898 nm	5 nm	387 nm
Inverted pyramids	958 nm	123 nm	383 nm
Gaussian circular diffusor	642 nm	168 nm	340 nm

derived from reflectance (R) and transmittance (T) measurements, as is shown in equation (1).

$$A = 1 - T - R. \tag{1}$$

Of particular interest is the wavelength region near the band gap of the perovskite, which is 1.68 eV. This corresponds to a photon wavelength of 738 nm. In this region, the influence of the texture beneath the perovskite layer can be seen. Compared to the planar reference sample, the textures with particularly high absorptance are the inverted pyramids and the periodic sinusoidal structure. Although the wavelength range near the bandgap is of particular interest, the textures also provide improved absorptance at nearly all wavelengths shorter than 738 nm. From finite-element method optical simulations on perovskite solar cells containing the sinusoidal and the inverted pyramidal texture we know, that the enhanced absorptance close to the perovskite bandgap arises from texture-induced light trapping in the perovskite layer, which can lead to up to 1 mA/cm^2 increased short circuit current density in the solar cell device [4]. In contrast, the use of a Gaussian diffusor texture seems to reduce the absorptance considerably. However, this is not due to unwanted optical effects or measurement errors, but to the fact that the perovskite did not form a uniform layer on this texture and that very large macroscopic holes were formed in the perovskite layer during spin coating

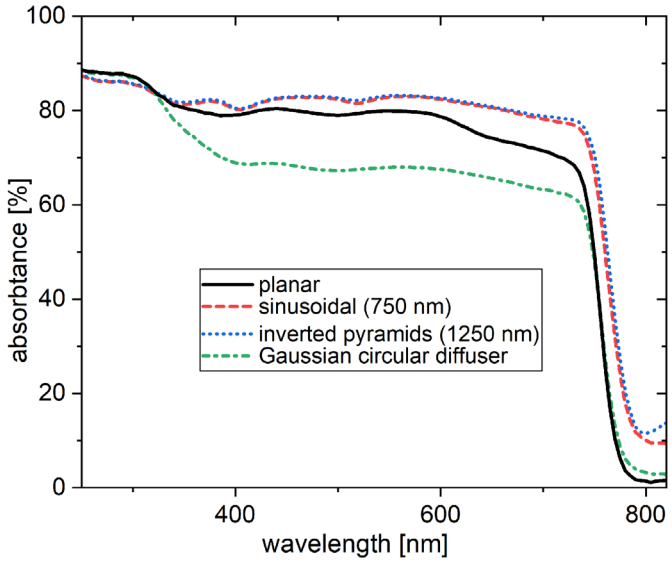

Fig. 7. Absorptance spectra of perovskite films spin-coated on the investigated textured glasses.

(see Fig. 6d). With an irregular perovskite layer, more of the light instead hits the glass, where it is either reflected or transmitted, but not absorbed to the same extent.

4 Conclusion

In this study, the growth process of perovskite layers via spin-coating from solution was investigated on differently textured substrates. Three different nanoimprint-textured glasses and planar reference glasses, all covered with an ITO layer and a hole transporting layer to mimic solar cell fabrication conditions, were used as substrates: A smooth sinusoidal and an inverse pyramidal structure with periodicities of 750 nm and 1250 nm, and structural heights of 300 nm and 500 nm, respectively. Further, a Gaussian circular diffusor structure with horizontal peak-to-peak distances in the range of several tens of micrometers and vertical feature of $1.6 \pm 0.2\,\mu$m. We monitored the perovskite spin-coating process using in-situ photoluminescence (PL). No significant differences in crystallization time, PL peak position, PL peak width or PL intensity were observed among the investigated sinusoidal and inverted pyramidal textured substrates compared to the planar reference. The much larger and random Gaussian circular diffusor texture varied especially in the measured PL intensity having a factor of roughly 7 lower intensity compared to all other textures. Scanning electron microscopy images revealed a homogenous growth of perovskite film on planar, sinusoidally textured, and inverted pyramidally textured substrates. In the case of the two textures (sinusoidal and inverted pyramids), the texture valleys were found to be well-filled with perovskite. In contrast, the larger diffusor texture yielded macroscopic holes in the perovskite film. Optical experiments showed an increased absorptance in the whole wavelength range below the electronic bandgap in films with sinusoidal and inverse pyramidal textures compared to a planar reference film. However, due to the observed macroscopic holes, the absorptance decreased in the perovskite film on the diffusor texture. We conclude, that within the set of investigated substrate textures the growth of a homogeneous and strongly absorbing perovskite film is possible for textures with horizontal and vertical features with a size of around one micrometer or smaller. In contrast, spin-coating perovskite onto a textured surface with vertical features larger than 1-2 µm resulted in non-uniform films with macroscopic holes. The results add new experimental data on in-situ growth of perovskite films on textured surfaces.

Funding

We thank the Helmholtz association for funding within the project "Zeitenwende - Accelerated transfer of the next generation of solar cells into mass production - future technology tandem solar cells". We further thank the Deutsche Bundesstiftung Umwelt (DBU) for funding within the TexturedTandem project (grant no. 37908/01), as well as temicon GmbH, Germany – for providing their commercial textured foils free of charge.

Conflicts of interest

The authors have no conflict of interests related to this publication.

Data availability statement

The data that supports the findings of this study are available from the corresponding author, Florian Riesebeck, upon reasonable request.

Author contribution statement

C.B. planned and supervised the project, F.M. supervised the experimental work, F.R. performed the measurements, processed the experimental data, performed the analysis, drafted the manuscript and designed most figures. S.T. performed the AFM measurements, D.Y. analyzed the AFM data and designed the designated figures. C.B., E.U., F.R. and F.M. aided in interpreting the results. C.B. aided in shaping the manuscript.

References

1. LONGi sets a new world record of 33.9% for the efficiency of crystalline silicon-perovskite tandem solar cells. Available from https://www.longi.com/en/news/new-world-record-for-the-efficiency-of-crystalline-silicon-perovskite-tandem-solar-cells/ (accessed on November 3, 2023)
2. B. Chen et al., Blade-coated perovskites on textured silicon for 26%-efficient monolithic perovskite/silicon tandem solar cells, Joule **4**, 850 (2020)
3. Y. Hou et al., Efficient tandem solar cells with solution-processed perovskite on textured crystalline silicon, Science **367**, 1135 (2020)
4. P. Tockhorn et al., Improved quantum efficiency by advanced light management in nanotextured solution-processed perovskite solar cells, ACS Photonics **7**, 2589 (2020)
5. P. Tockhorn, J. Sutter, A. Cruz et al., Nano-optical designs for high-efficiency monolithic perovskite-silicon tandem solar cells, Nat. Nanotechnol. **17**, 1214 (2022)
6. M. De Bastiani et al., Monolithic perovskite/silicon tandems with >28% efficiency: role of silicon-surface texture on perovskite properties, Adv. Funct. Mater. **33**, 2205557 (2023). https://doi.org/10.1002/adfm.202205557
7. A. Al-Ashouri et al., Wettability improvement of a carbazole-based hole-selective monolayer for reproducible perovskite solar cells, ACS Energy Lett. **8**, 898 (2023)

8. K. Hossain, A. Kulkarni, U. Bothra, B. Klingebiel, T. Kirchartz, M. Saliba, D. Kabra, Resolving the hydrophobicity of the Me-4PACz hole transport layer for inverted perovskite solar cells with efficiency >20%, ACS Energy Lett. **8**, 3860 (2023). https://doi.org/10.1021/acsenergylett.3c01385
9. A. Farag, T. Feeney, I.M. Hossain, F. Schackmar, P. Fassl, K. Küster, R. Bäuerle, M.A. Ruiz-Preciado, M. Hentschel, D.B. Ritzer, A. Diercks, Y. Li, B.A. Nejand, F. Laufer, R. Singh, U. Starke, U.W. Paetzold, Evaporated self-assembled monolayer hole transport layers: lossless interfaces in p-i-n perovskite solar cells, Adv. Energy Mater. **13**, 2203982 (2023). https://doi.org/10.1002/aenm.202203982
10. A. Kulkarni et al., A universal strategy of perovskite ink − substrate interaction to overcome the poor wettability of a self-assembled monolayer for reproducible perovskite solar cells, Adv. Funct. Mater. **33**, 2305812 (2023). https://doi.org/10.1002/adfm.202305812
11. P. Holzhey et al., Understanding the impact of surface roughness: changing from FTO to ITO to PEN/ITO for flexible perovskite solar cells, Sci. Rep. **13**, 6375 (2023). https://doi.org/10.1038/s41598-023-33147-6
12. W. Wang et al., Wet-chemical surface texturing of AZO substrate for improved perovskite solar cells, J. Alloys Compd. **963**, 17110 (2023). https://doi.org/10.1016/j.jallcom.2023.171105
13. A. Magomedov, A. Al-Ashouri, E. Kasparavičius, S. Strazdaite, G. Niaura, M. Jošt, T. Malinauskas, S. Albrecht, V. Getautis, Self-Assembled Hole Transporting Monolayer for Highly Efficient Perovskite Solar Cells, Adv. Energy Mater. **8**, 1801892 (2018)
14. M. Saliba et al., Cesium-containing triple cation perovskite solar cells: improved stability, reproducibility and high efficiency, Energy Environ. Sci. **9**, 1989 (2016). https://doi.org/10.1039/C5EE03874J
15. A. Merdasa, C. Rehermann, K. Hirselandt et al., Eye in the process: Formation of "triple cation" perovskite thin films rationalized by in-situ optical monitoring (2020), Available at Research Square. https://doi.org/10.21203/rs.3.rs-102041/v1
16. F. Mathies, E.R. Nandayapa, G. Paramasivam, M.F. Al Rayes, V.R.F. Schröder, C. Rehermann, E.J.W. List-Kratochvil, E.L. Unger, Gas flow-assisted vacuum drying: identification of a novel process for attaining high-quality perovskite films, Mater. Adv. **2**, 5365 (2021)
17. M. Lv, X. Dong, X. Fang, B. Lin, S. Zhang, J. Ding, N. Yuan, A promising alternative solvent of perovskite to induce rapid crystallization for high-efficiency photovoltaic devices, RSC Adv. **5**, 20521 (2015)

Cite this article as: Florian Riesebeck, Florian Mathies, Danbi Yoo, Sergei Trofimov, Eva Unger, Christiane Becker, Investigation of perovskite layer growth from solution on textured substrates, EPJ Photovoltaics **15**, 19 (2024)